

# Challenges in Static Testing of Co-Cured Co-Bonded Composite Aircraft Structures

**B. Ramanaiah\*, H.V. Ramachandra, S. Sanjeev Kumar, M.G. Kotresh, Byji Varughese, Ramesh Sundaram, G.M. Kamath and M. Subba Rao**

Advance Composites Division, National Aerospace Laboratories, Bangalore-560017, INDIA

E-mail: \*ramanaia@nal.res.in

## ABSTRACT

*Due to several advantages, advanced composite structures have been successfully used for developing several primary aircraft structures. One of the certification requirements, as per FAR 25, is to ensure their compliance to the design loads by conducting static tests. Based on the requirements given by the designer, the experiments are conducted. To achieve realistic behavior of the structure in the static test loading and attachments should be properly simulated. This requires considerable time and is a very challenging assignment. The general philosophy is to carryout limited testing, and then uses analytical models to simulate other load cases. A good correlation between testing and analysis is essential to gain confidence in the design of the structure. The total aerodynamic loads are to be distributed as lumped loads without effecting much change in the bending moments and shear forces diagrams. Testing also involves collection of reliable information from strain gauges, dial gauges and acoustic emission sensors. Adequacy of the test rigs and proper simulation of all attachments need to be addressed. The design of the whiffletree to distribute the loads in the desired fashion is one of the key parameters in the testing process. The paper discusses these aspects and the challenges in carrying out static test through a few examples.*

**Keywords:** Wing Test Box, Static Testing, Out Board Flap, Elevator, Cyclic Load Testing.

## 1. INTRODUCTION

Existing primary aircraft structures are typically fabricated by fastening the skins to the internal substructure comprising of spars and ribs. The limitations of this type of construction are: (i) high production time and assembly cost (ii) increased weight penalty (iii) maintenance issues like leakage, loosening of fasteners. Advanced composite aircraft structures fabricated using co-cured/co-bonded techniques eliminate these limitations to a great extent. The skin, rib and spar are co-cured or co-bonded to develop the substructure. The primary structures like fin, rudder and control surfaces are manufactured using this technique. In order to demonstrate the feasibility of co-cured wing for a military aircraft, at NAL a wing test box was designed and fabricated. The structural integrity of the box was

proved through static test at room temperature and at hot-wet condition. On the other hand, testing the structure in hot-wet conditions is tedious and is not always feasible. In such situations the integrity of the structure is proved at a load higher than the Design Ultimate Load (DUL). Such an approach is used in the case of control surfaces like elevator. The aft box of control surface structures like flaps is fabricated with co-bonding of aft akin and aft ribs. In these structures the skin to rib debonding may occur during fabrication or in the service due to impact. The integrity of the structure at cyclic load is a concern to the designer. The outboard flap of a civil aircraft which had multiple debonds at the skin-rib interfaces, has been subjected to cyclic loading. Test set up for all the above types of requirements are quite complex and challenging. The load distribution, design of whiffle tree set up and the monitoring of output are

all important to conduct a successful test. In this paper these aspects are discussed in detail based on the authors' experience on some of the important tests at NAL.

## 2. WING TEST BOX

The wing test box is designed for static loads in room temperature (RT) and hot-wet (HT) conditions. The geometry of the test box is shown in Fig. 1. The test box is about 1.6 m in length, 1.2 m in width and 236 mm in height. The structure consists of metallic and CFC (carbon fiber composite) components. The carbon fiber composite components are the spars, ribs, and skins. The thickness of the skins varies from around 16mm to 6mm. The metallic components include the root fittings, shear bracket, part of the auxiliary root rib (mid portion), and the fasteners. Spars 11 (11A and 11B), 12 (12A and 12B) and 13 (13A and 13B) and the Pylon Rib are co-cured with the bottom skin as shown in Fig. 2. A view of the partially assembled box is shown in Fig. 3.

### 2.1 Design Loads

The test box representing a portion of the wing is expected to withstand mainly the forces of: bending moment ( $M$ ), torsional moment ( $T$ ), and shear forces ( $S$ ). The design ultimate loads are equal to 1.5 times the limit load which corresponds to the maximum up bending moment maneuvering load case. In view of the single fitting option chosen for the present design, the root fitting can be expected to withstand only the bending moment and the shear force while the box takes all the three loads. The magnitudes of the loads P1, P2, P3, P4 and P5 are 23000, 23000, 12000, 70000, and 58000 (in Newton) respectively. P1 and P2 are applied at the ends of the root rib. P1 is applied at the end near Spar 10 (root rib fwd) in the positive (up) direction and P2 at the end near Spar 14 (root rib aft) in the negative (down) direction. P3 is applied on the loading rib at the end near Spar 10 and P4 is applied on a loading bracket fixed to the loading rib below Spar 12B. P5 is applied on the loading rib near spar-14. P3, P4 and P5 are applied in the positive (up) direction.

### 2.2 Room Temperature Testing of the Wing Test Box

The test box was mounted on a test rig by means of a special root fitting attachment fixture that connects the root fitting to the test rig. The static loads were applied

at the loading points by means of hydraulic jacks using load cells. Dial gauges and strain gauges were used to monitor the deflections and the strains, respectively. The test box was extensively instrumented with the strain gauges. The loads were applied in steps of 10% of the limit load, and the corresponding strains and deflections measured. Fig. 4 shows the test box mounted on the test rig with the loading rib jacks visible in the picture. In order to simulate the fuel pressure in the wing test box, arrangements were made to seal the box and apply a pressure of 7 psi. The aim was to apply the static load and the internal pressure simultaneously.

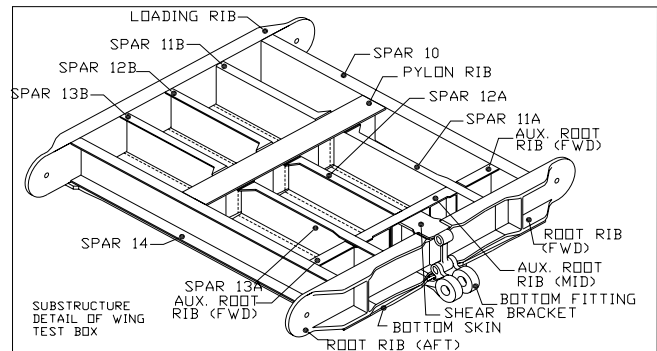


**Fig. 1: Geometry of the Wing Test Box**

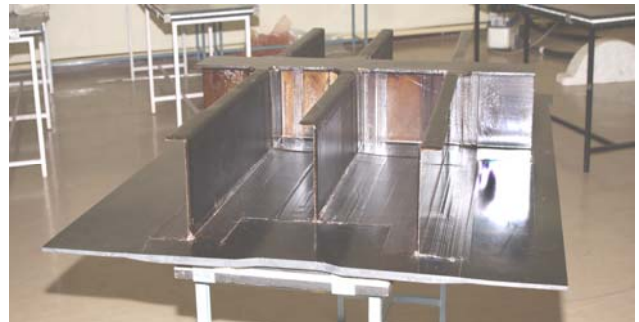


**Fig. 2: A Photograph of the Co-cured Substructure**



**Fig. 3: A View of the Partial Assembly of the Wing Test Box**

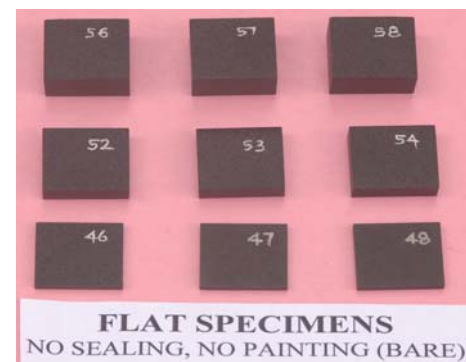


**Fig. 4:** The Co-cured Wing Test Box being Statically Tested Under Room Temperature Conditions

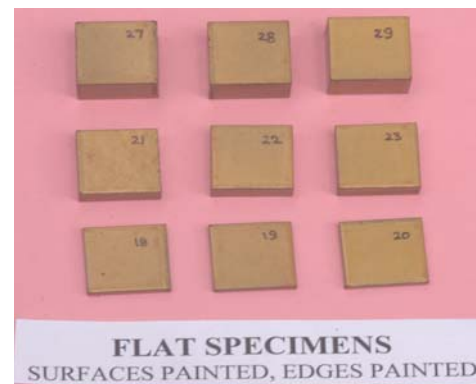
### 2.3 Environmental Conditioning

The box was placed in an environmental chamber that was maintained at 85% RH and 70 deg C for conditioning purpose. The normal procedure for specimen level and feature level environmental conditioning is that they are removed periodically and weighed, and the moisture content is determined from the weight increase from the dry specimen. However, this procedure is not practical for a box so large and heavy. Nevertheless, it is important to ensure that the box is completely saturated with moisture in the as-assembled condition because it is exposed to the ambient conditions in the field in this assembled condition. Usually, specimen conditioning is done in the as-fabricated condition. But, in the actual case, paints or sealants are usually applied on airframe components. Moreover, typically an airframe component is of varying thickness in different regions, as in the case of the test box. Thus, these factors should be taken into account while conditioning. In order to study the effects of the above mentioned factors, different specimens and features were placed in the environmental chamber along with the test box. The specimens and features fabricated were flat specimens, T-joints and boxes. The flat specimens were 25 mm × 25 mm in size with varying thickness of 3.6 mm, 9 mm and 15.9 mm. Among the flat specimens, for each thickness, four sets were fabricated: (i) One set was sealed at the edges to prevent moisture absorption through the edges and the faces were bare, (ii) One set was painted on the faces and sealed on the edges, (iii) One set was painted on the faces and the edges, and (iv) One set was totally bare, i.e., it was neither painted nor sealed. The paint used here was the standard epoxy yellow primer used in the aircraft industry. The sealing was done using the PR-sealant 1422. The bare specimens and the painted

specimens are shown in Fig. 5, respectively. T-joints were also fabricated and conditioned along with the test box. The schematic and the photographs are shown in Fig. 6 respectively. In addition to the flat laminates and T-joints, two sets of boxes were also fabricated and placed in the chamber. These were of the size 50 mm × 50 mm × 56 mm and of thickness 9 mm. One set was completely closed (Fig. 7). This was to study if the complete sealing of the box results in lower levels of moisture absorption. Another set had two holes of 10mm dia on two faces to allow for moisture to be absorbed from the inside of the box. Each of these specimens and features were periodically removed (once a week) and weighed and the moisture content noted. This was done until saturation in the moisture levels of all the features and specimens were observed, which took approximately 14 months. The comparisons of the moisture absorption rates for the flat specimens of thickness 9 mm and 15.9 mm with different treatments



(a)



(b)

**Fig. 5:** Flat Specimens that were Saturated along with the Box. (a) Bare Specimens, (b) Painted Specimens. Each Row is a Specimen of Varying Thickness (from top to bottom, 3.6 mm, 9 mm and 15.9 mm)

are shown in Fig. 8 and 9, respectively. It can be seen that the treatments do not substantially affect the rates. The effect of thickness of the specimens is shown for the bare specimens in Fig. 10. The thinner specimens absorb moisture at a faster rate than the thicker specimens although the saturation levels are the same. The moisture absorption rates for the box specimens and the T-joints are plotted in Fig. 11. The T-joints absorb moisture at a faster rate and also saturate at a higher level. The open box also absorbs moisture faster and saturates a level marginally higher than the closed box.

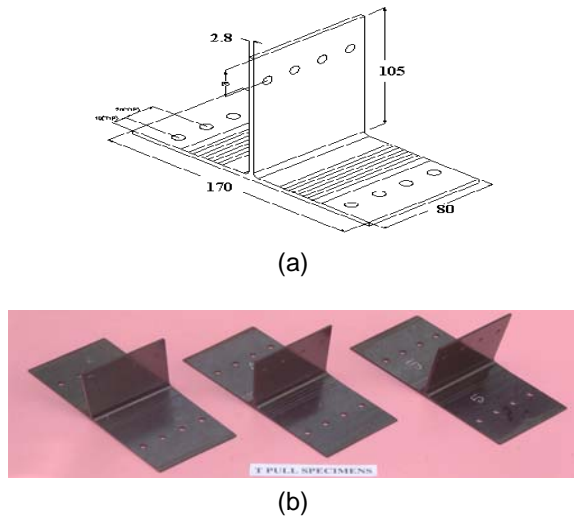


**Fig. 6 (a):** Schematic of T-joint that was Saturated with the Box (dimensions in mm). The Base Skin Thickness is 3.6 mm, (b) Photographs of the T-joints

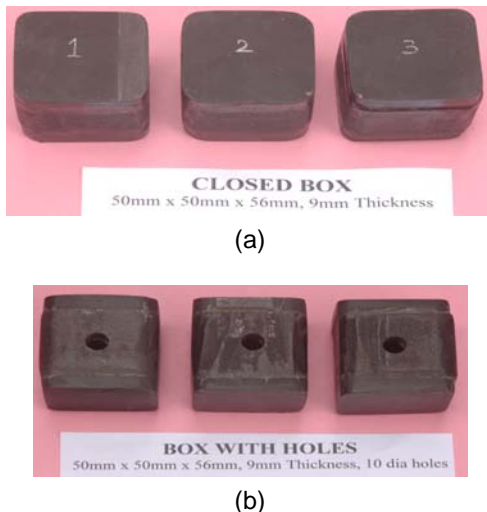


**Fig. 7:** Box Specimens Saturated along with the Box. (a) Completely Closed Box, (b) Box with 10 mm Dia Holes on Two Faces to Allow for Moisture Absorption Through Inside Surfaces

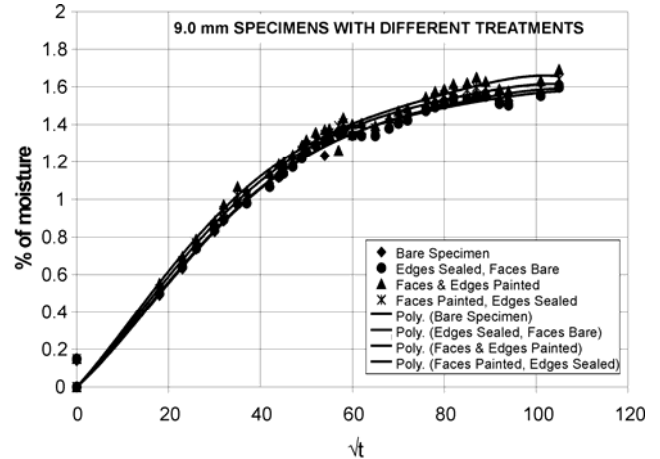


**Fig. 8:** Moisture Absorption Rates for 9 mm Specimens with Different Treatments

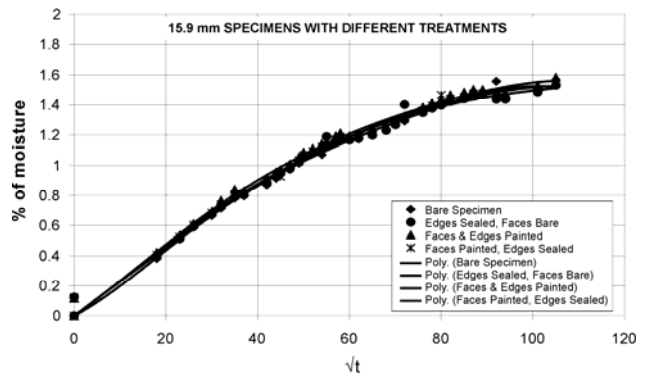


**Fig. 9:** Moisture Absorption Rates for 15.9 mm Specimens with Different Treatments

After the test the moisture gained, T-joints and boxes the plot specimens were kept in a room temperature environmental and periodically weighed and moisture content was noted. Similarly, the moisture losses was monitored up to 1500Hours and Fig. 14 shows the a continuous decrease in the moisture content.

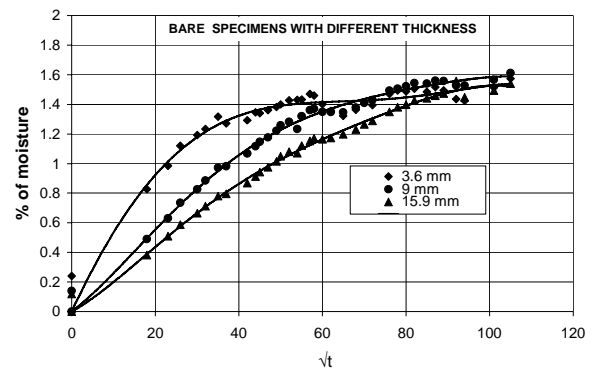


**Fig. 10:** Moisture Absorption Rates for Bare Specimens



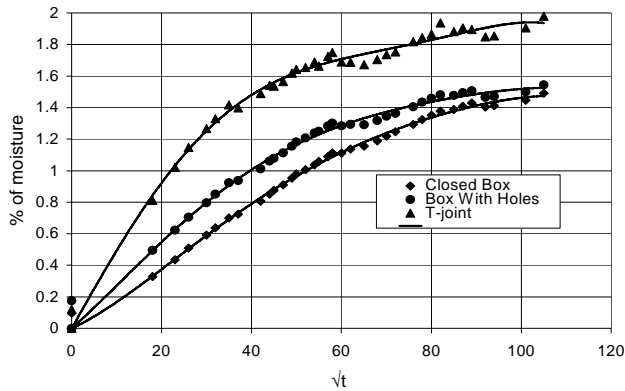


**Fig. 11:** Moisture Absorption Rates for Box and Joints



**Fig. 12:** Flexible Bagging Around the Box for the Steam



**Fig. 13:** Wing Test Box Enclosed in the Bag and the Insulating Outer Box

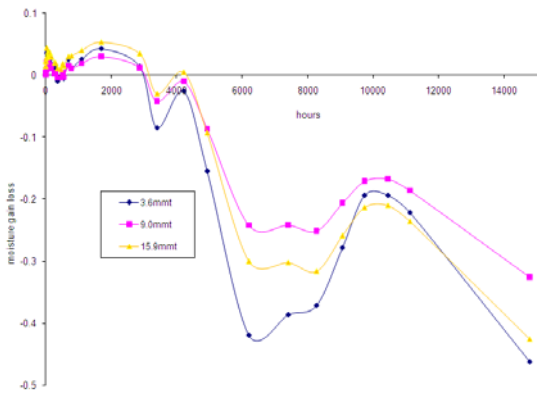


**Fig. 14:** Moisture Losses for Without Painting and Sealing Specimen

### 3. OUT BOARD FLAP CYCLING TESTING

#### 3.1 Test Article

Outboard flap of SARAS aircraft is a chambered aerofoil structure with skin-rib-spar construction. It is fabricated with unidirectional carbon fiber prepreps. It has a nose box, a aft box, 10 chordwise I-section ribs and one c-section spar along the span. Exploded view of flap is shown in Fig. 15 and cross section of flap is shown in Fig. 16. The nose box, nose ribs and spar are fastened using rivets. The aft ribs are bonded to the aft skins using Redux 319 adhesive. The aft box assembly along with ribs is fastened to the spar using rivets. The secondary bonding between the aft skins and aft ribs are of the importance in this paper. Detailed A-scan, after the fabrication, revealed discontinuities in the bonding between ribs and aft box skin. Some regions are weak bonds and some regions are clear debonds. This test article was subjected to limit and ultimate load tests. Component withstood ultimate load successfully without any failure. Later detailed A-scan and thermo graphic scanning were carried out on the structure before starting the damage tolerance test. Fig. 17 shows the flap with initial debonds.

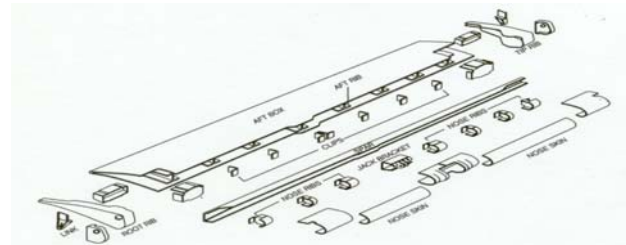


**Fig. 15:** Exploded View of SARAS out Board Flap



**Fig. 16:** Cross Section of the Flap

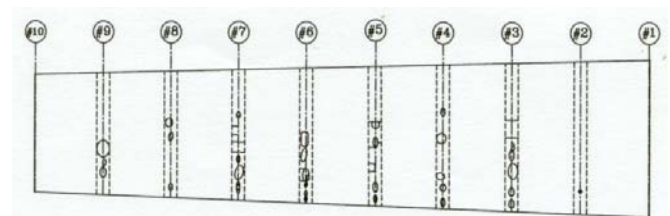


**Fig. 17:** Debond on the Flap before the Test

### 3.2 Aero Dynamic Load

The magnitudes of suction, pressure and chord wise loads are 394 kgs., 213 Kgs. And 106 Kg. respectively. The pressure and chordwise loads are distributed as concentrated loads at each rib location. The suction is also distributed as lumped loads to act between the ribs. This is done intentionally to avoid fouling between suction and pressure loading members. The suction and pressure loads at each rib were further divided into two loads such that their resultant lies on the center of pressure (c.p). Fig. 18 shows the all load locations on the flap.

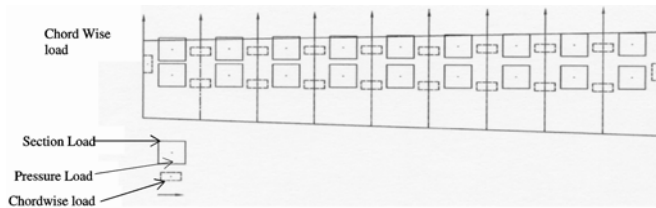


Fig. 18: Load Location on the Flap

### 3.3 Loading Mechanism

The total aerodynamic load was redistributed as 46 concentrated loads (suction–18, pressure –18 and chord wise–10) for the purpose of structural testing. At least three actuators would be needed to apply suction, pressure and chord wise loads separately through independent whiffle tree systems. But, as all the loads must be applied simultaneously, synchronization of three actuators would become very difficult in cyclic loading. There should not be any phase lag between the actuators. To satisfy this condition, a special whiffle tree loading mechanism has been designed to reduce all the 46 loads to a single actuator. Pressure load at one rib is connected to the adjacent suction load. Chord wise load in the chord line direction is changed to normal direction through pulleys. Finally all the loads are carefully connected to actuator by avoiding fouling between the whiffle tree loading members. Fig. 19 shows the whiffle tree arrangement. Pressure loads are applied using the wooden pads (with rubber lining). Special canvas pads are prepared and bonded to the flap surface to connect suction and chord wise loads.

### 3.4 Simulation of Attachment Conditions

The flap is mounted to the wing by means of two roller points, two link points and a jack point. The aerodynamic load that acts on the flap reacts at all five

points in specific directions. The direction of these reactions depend on deployment position of the flap. Test is conducted for 30 deg. deployment case. The flap along with all the boundary conditions was rotated by 30 deg. in anticlockwise direction for the convenience of the testing. Flap is constrained at the roller points. Load cells are placed in the link rods to monitor the reactions. Fig. 20 shows the schematic view of the simulated test set up.

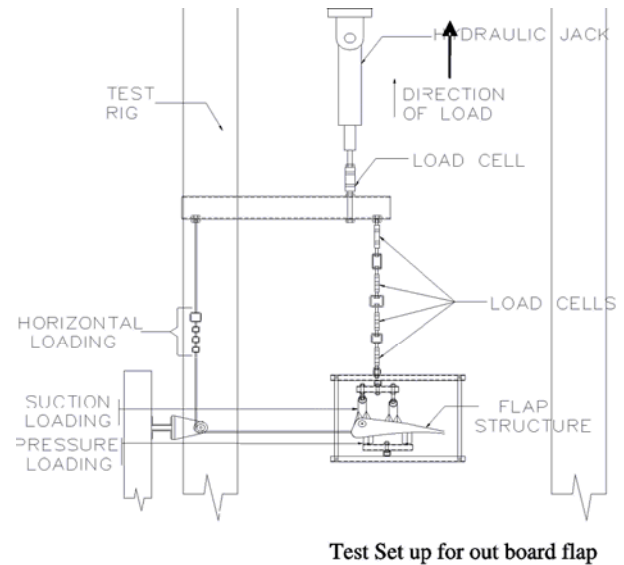


Fig. 19: Whiffletree Arrangement for Flap

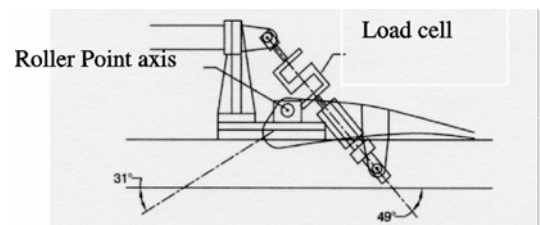


Fig. 20: Simulated Test Set Up

### 3.5 Testing

Cyclic load is applied on the flap using whiffle tree loading mechanism and a hydraulic jack. A load cell used to monitor the applied load. Component was loaded at very low frequency because of number of loads, complex loading and power pack limitations. Resistance strain gauges are mounted on the debonded region to study the variation of the strains during the propagation of Debonds. Few gauges are also mounted on the healthy regions (very close to the Debonds) to observe the change in strain when debond grows. 100 channel data logger system is used to monitor the strains in the structure. One dial gauge is used to study the variation in the global stiffness of the structure during the test. Two optical strain gauges are mounted to acquire real time strain data from the component. Acoustic emission sensors are placed to capture the real time data of acoustic activity in case of damage growth or initiation. Fatigue load equal to design limit load (712 Kg) is applied on the component for the test. Minimum and maximum loads are 200 and 712 Kg. respectively. Damage growth was assessed using ultrasonic A-scan after every 1000 load cycles. Strains and deflections were monitored under static load after every 1000 cycles.

### 3.6 Results

The debonds in the skin to spar interface have not shown any growth till 25000 load cycles. Later these debonds started growing slowly at various locations. Ultrasonic A-Scan revealed growth in debonds between some cycle blocks (1 cycle block = 1000 cycles). However it is found that the growth of debonds at any location is not continuous i.e., once the growth is noticed for any debond after one cycle block, further growth is not seen continuously in the next cycle blocks. Different debonds have grown by different magnitudes in different cycle blocks. Fig. 21 shows the strain plot of gauges 1 and 5 which were mounted on the debonds. Changes in strain could not be seen though these debonds have grown slightly during the test. Fig. 22 shows the strain plot of strain gauges 13 and 18 which were mounted on well bonded region, but close to the debonds. These debonds also have grown during the test but did not grow till the strain gauge. The strains of these gauges also have not changed as the growth is very small.

Thermography images were taken at each rib before the test and after 2-lack load cycles. Fig. 23 shows

thermography images for rib 3 before and after the test. Thermography report at each rib is in good agreement with the ultrasonic A-scan report. Acoustic emission sensors are used to monitor the real time acoustic activity in the structure. It helped in the on-line assessment of damage initiation/growth and its intensity.

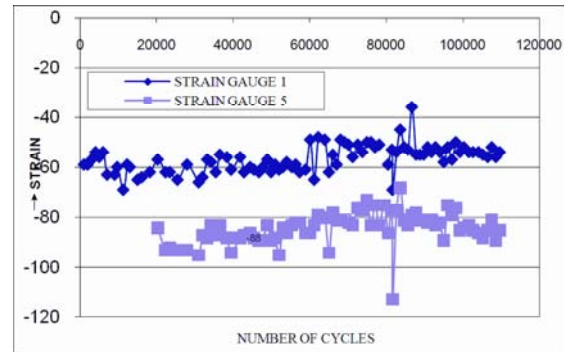


Fig. 21: Strain Plot of Strain Gauge 1 and 5

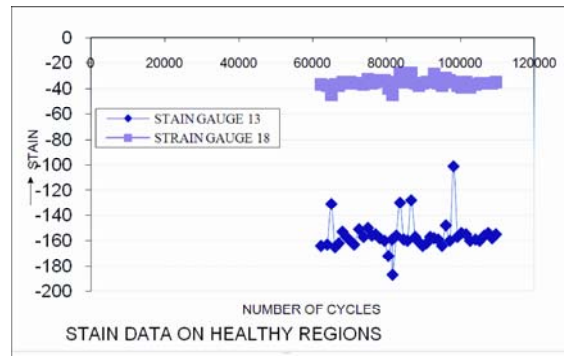
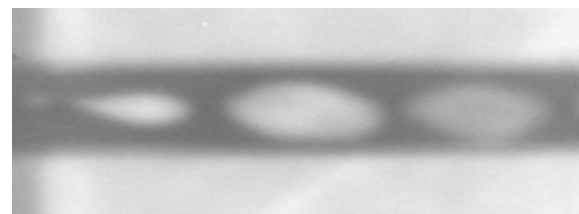
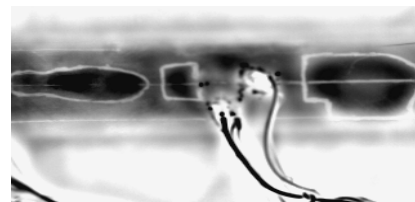


Fig. 22: Strain Plot of Strain Gauge 13 and 18



(a) Before The test



(b) After The Test

Fig. 23: Thermography Images at Rib 3

Fig. 24 shows acoustic activity near a de-bond during one cycle block. A-scan report after 1000 cycle block has always revealed some damage growth around Acoustic Emission (AE) sensor vicinity, where significant Acoustic Emission (AE) activity has been noticed.

The deflection of flap under static load is monitored using a dial gauge. The deflection of the flap at the trailing edge was increased by 1mm during the span of test, indicating some loss in the stiffness of the structure.

## 4. ELEVATOR STATIC TESTING (LH)

### 4.1 Limit Load Test of Elevator

To demonstrate the structural integrity of the elevator, the elevator was subjected to static test. A test rig with adequate stiffness was specially designed and fabricated for elevator testing. Initial checks were made to ensure there is no rigid body displacement. The Geometry of the elevator shown in Fig. 25 The elevator is mounted to the horizontal stabilizer by means of three hinges namely Inboard hinge, mid hinge and

Outboard hinge. All these supports are simulated in the static testing by suitable fixtures. The Inboard hinge of the elevator attached to the torque tube of the elevator just as it is mounted on the aircraft. Thirteen Load stations were selected for applying load and total aerodynamic load of 520 Kgs (limit load) into 24 places .Pad locations were marked on the elevator and Fig. 26 shows the pad locations. Dial gauges were mounted on leading edge, spar line and trailing edge. The exact locations for the measurement of deflections were shown in the Fig. 27. Foil type strain gauges supplied by Kyowa, Japan were mounted on the skin and attachment portions. The location of the strain gauges were given in the Fig. 28. Load was applied top surface of the elevator using lead shot bags simultaneously RH simulated loads also applied using suitable mechanism with dead weights and jacks. During loading and unloading strains, deflections and torque tube link reaction were measured during the test. The photograph Fig. 29 shows the elevator undergoing limit load test.

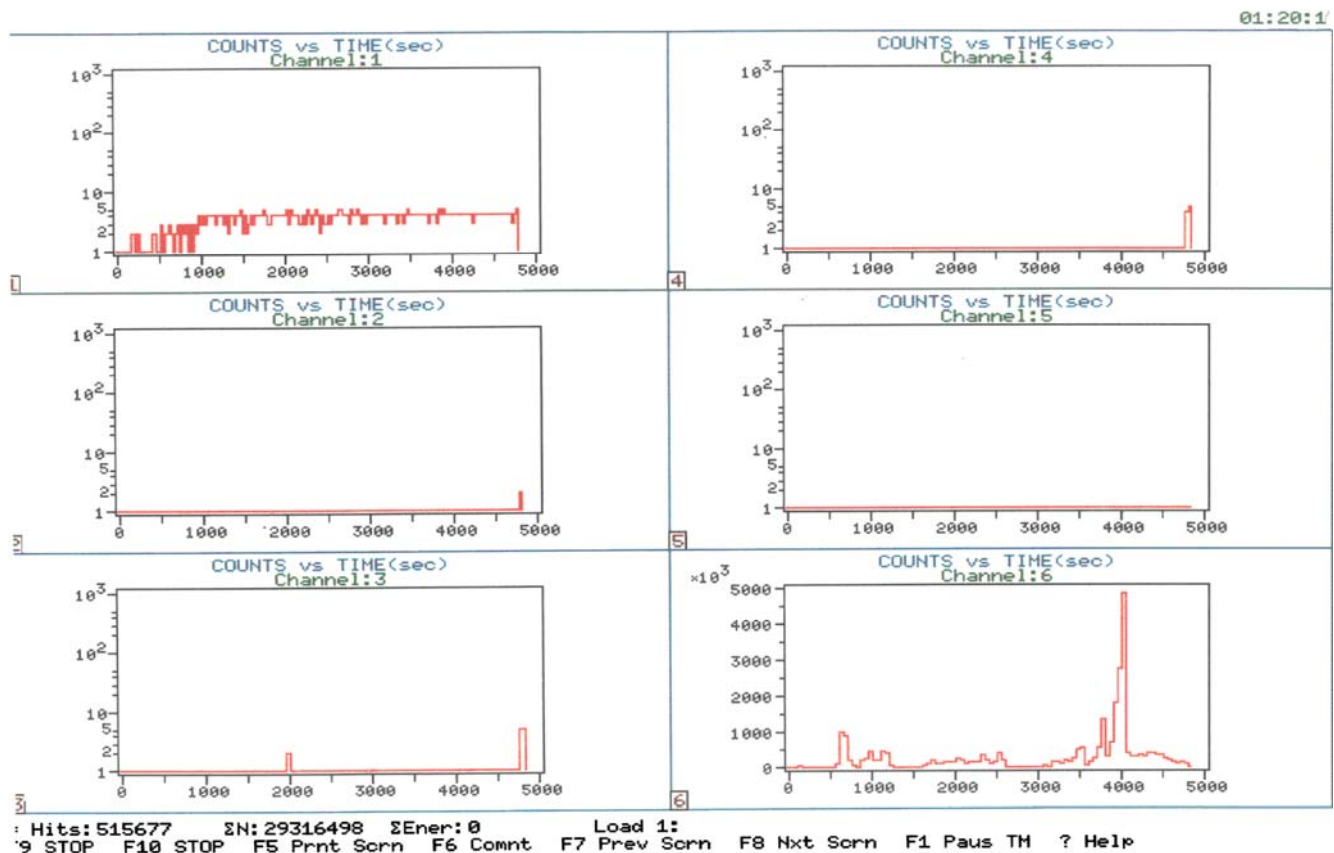


Fig. 24: AE Data from Various Sensors during the Test



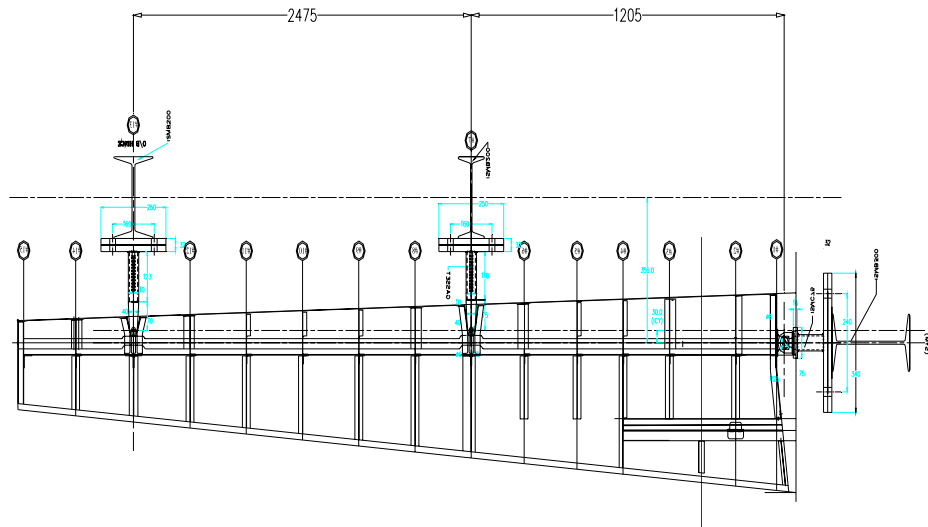


Fig. 25: Geometry of the Elevator

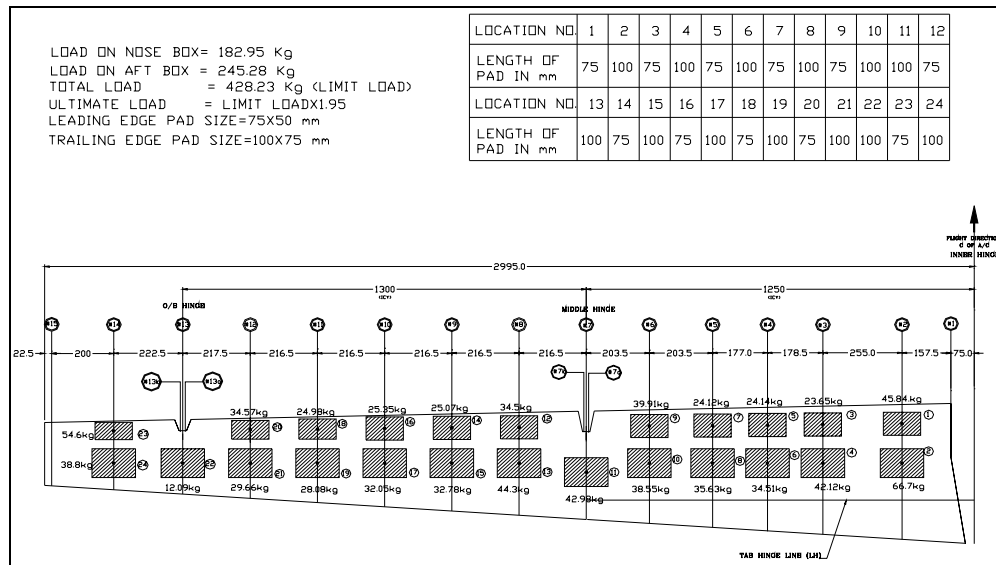


Fig. 26: Pad Location of Elevator

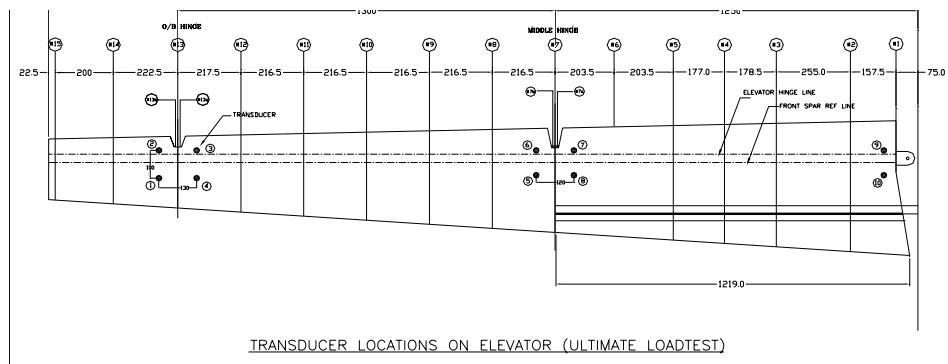
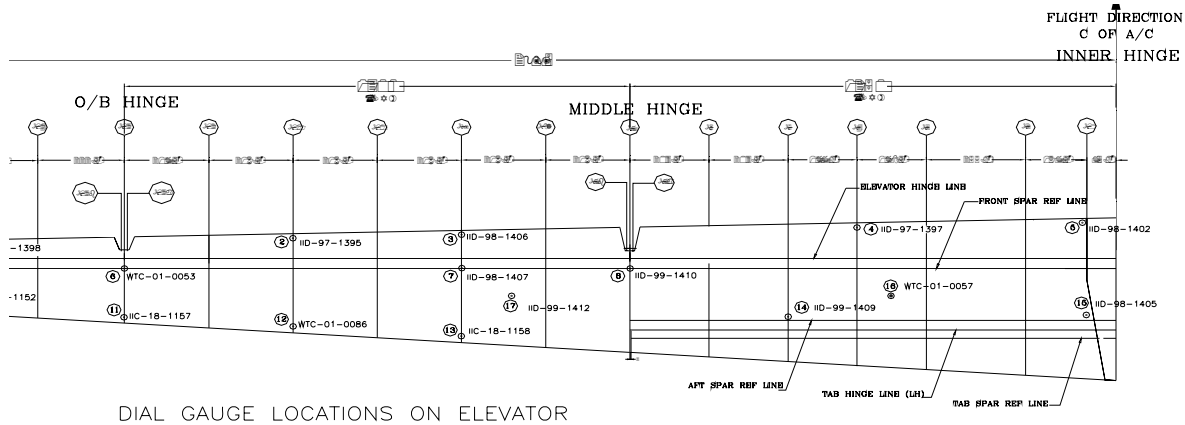


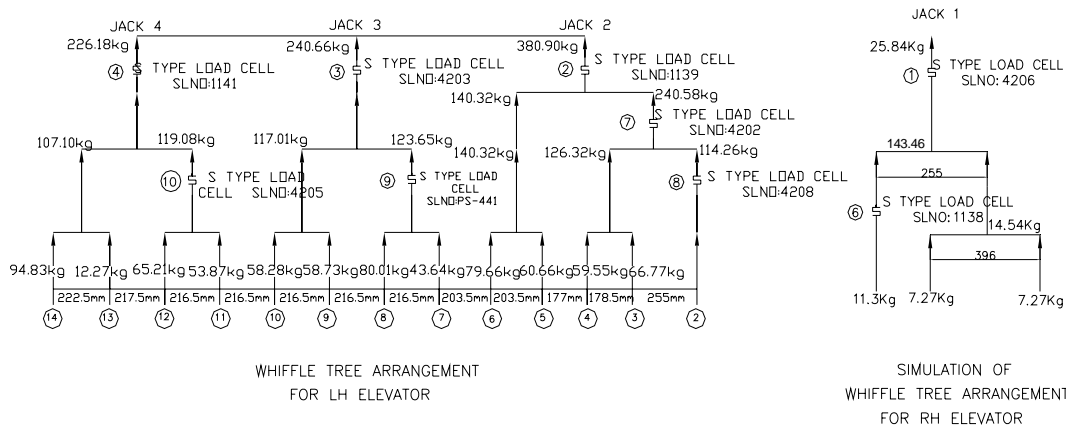
Fig. 27: Strain Gauge Locations for Elevator LH



DIAL GAUGE LOCATIONS ON ELEVATOR

DIAL GAUGES 16&17 MEASURES DEFLECTIONS ON LOADED SURFACE

**Fig. 28: Dial Gauge Locations for Elevator LH**



WHIFFLE TREE ARRANGEMENT  
FOR LH ELEVATOR

SIMULATION OF  
WHIFFLE TREE ARRANGEMENT  
FOR RH ELEVATOR

**Fig. 30: Line Diagram for Whiffle Trees**

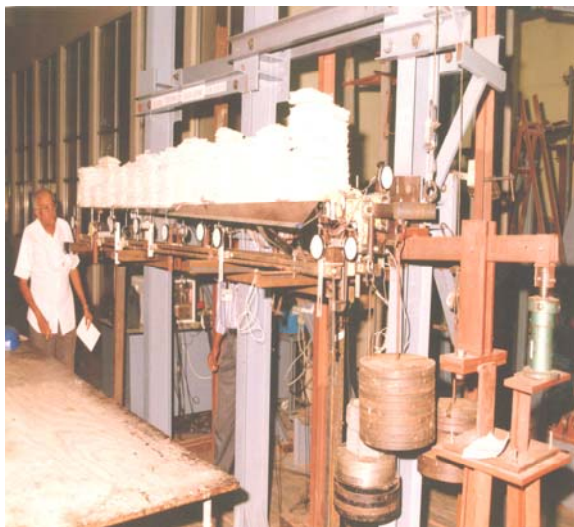


**Fig. 29: Elevator LH Undergoing to 100% of Limit Load Test**

## 4.2 Ultimate Load Test of Elevator

The whiffle tree loading system is designed for various loads and reactions that are expected during the static test of elevator. The line diagram of whiffletree shown in Fig. 30. The test loads are applied through 3 jacks. The loads that are coming on the whiffle tree members are monitored using load cells at 7 locations. The directions of jack loads are such that the test loads at different stations will be acting on bottom side of the elevator in the upward direction. Simulation for the reaction & torque from the RH elevator is done by providing a suitable mechanism on the right hand side of the torque tube of elevator. The whiffle tree member, loading jacks and calibrated load cells were assembled in their respected positions. The loads were applied gradually in steps of 10% through the whiffle tree upto 198% of the limit load and unloaded to zero. The torque tube link reaction measured using a load cell during the

test. The deflections and the strains were monitored during loading and unloading. The photograph shows the elevator is undergoing ultimate load test.



**Fig. 31:** SARAS LH Elevator Undergoing Static Testing 198% of Limit Load

## 5. WING TEST BOX STATIC TESTING

### 5.1 Geometry of the Wing Test Box

Composite test box (SARAS Composite wing) is basically a cantilever box beam structure with dimensions equal to  $1140 \times 275 \times 2050$  mm (width  $\times$  height  $\times$  span). Box contains top and bottom skins to take global bending and inplane shear, two spars to take transverse shear and six ribs to resist differential displacements between two spars at various sections of the box and also to prevent skin and spar buckling. The Geometry of the top skin and bottom skin are shown in Fig. 32(a) & 32(b) respectively.

### 5.2 Load

The test loads on the box are simulated at station #7, #8, #9 (vertical shear loads) and at station #10 (moment generating loads). The vertical shear loads are applied at the front spar and rear spar through load pads. The moment generating loads are applied in the horizontally through five metallic loading brackets. The box will be tested for the major flight load cases viz. 1. Flap down case, 2. Maximum down case, and 3.  $V_D$  case.

### 5.3 Testing of Wing Test Box

Suitable test rig and mounting fixtures designed fabricated and installed. The component was mounted on the test rig along with the mounting fixture. Strain

gauges, dial gauges and Acoustic emission (AE) sensors were fixed on the component. Figs. 33–35 show the locations respectively. Load was applied for bending moment generating loads at Inboard and Outboard at #10 are 3034.5 kg and 3034.5 kg respectively and Shear Loads at front spar at #7, #8, #9 are 814.59 kg, 2223.46 kg, 2970.38 kg and rear spars at #7, #8, #9 are 2366.26 kg, 1094.51 kg, 3155.30 kg respectively using the hydraulic jacks and calibrated load cells in steps of 10% limit load till the design ultimate load reached. Monitored the strains, deflections and Acoustic emission (A.E). output at every load step. Unloaded the structure in steps of 10% limit load to zero load. Monitored the strains, deflections and Acoustic emission (A.E). output at every unloading steps. The photograph in Fig. 36 shows the component undergoing Static testing.

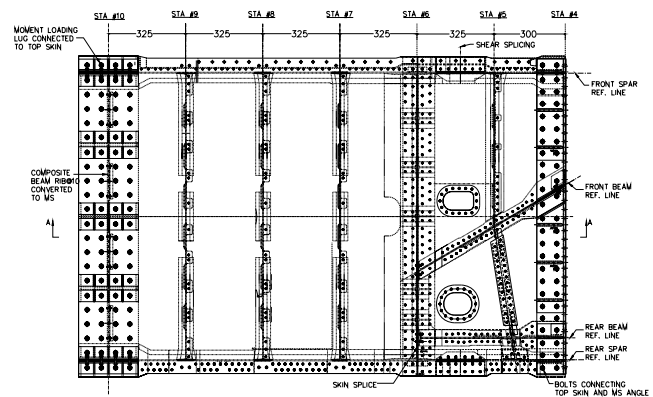


**Fig. 32(a):** Schematic Diagram of Wing Test Box-Top View

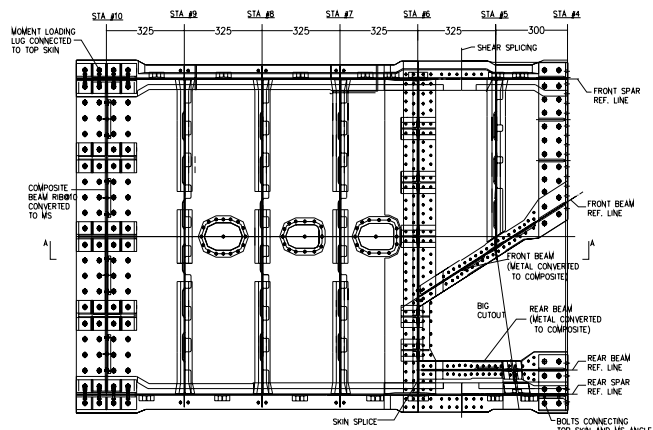


**Fig. 32(b):** Schematic Diagram of Wing Test Box-Bottom Skin

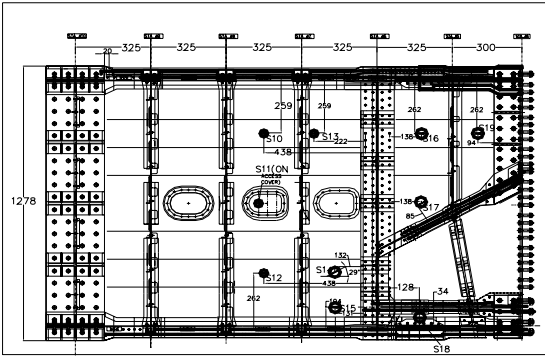


Fig. 33: Strain Gauges on Bottom Skin

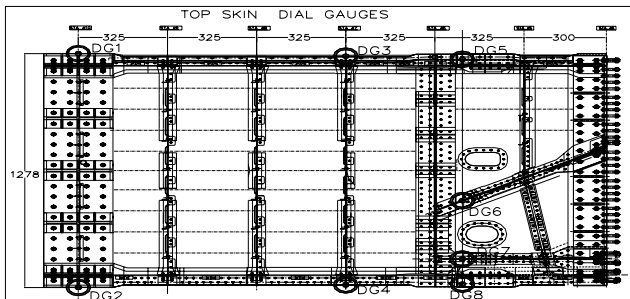


Fig. 34: Dial Gauges on Top Skin

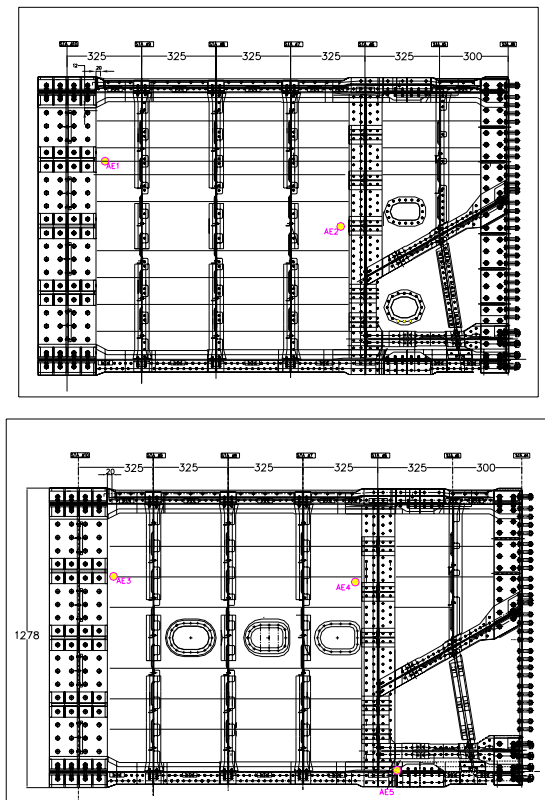


Fig. 35: Location of Acoustic Emission Sensors  
Top Skin & Bottom Skin



Fig. 36: Wing Test Box Undergoing Static Test

## 6. CONCLUSIONS

A co-cured composite test box was designed, fabricated and tested. The objective of this study is to closely examine the feasibility of fabricated a large and complex structure such as a main root box of an aircraft using co-curing technology. The results of the static testing done under room temperature and hot-wet conditions are presented here. In order to conduct the hot-wet tests for such a large structure, a rational and systematic approach was conceived and applied. Specimens and features were placed along with the box in the environmental chamber for conditioning. Different treatments such as sealant and paint were applied on the specimens to study the effect of these in the moisture absorption rates. It was found that the treatments had no substantial effect on the rate or percentage of moisture absorption. To examine the effect of having a box construction on the moisture absorption, closed and open boxes were fabricated and conditioned with the test box. T-joints were also conditioned with the test box. These specimens and features were periodically inspected for the moisture content and upon their saturation the test box was tested. A special chamber using a combination of flexible bagging and insulating box structure was fabricated around the test box. Steam generators were fabricated and used to generate the steam that maintains both the humidity and temperature. The results of the hot-wet testing have shown that there is no appreciable change in the stiffness of the test box. Under these conditions, the test box was tested up to 200% of the limit load. The box was then inspected using ultrasonic scanning and it was found that the co-cured joint areas in the substructure were intact. This study thus clearly demonstrates the feasibility of fabricated a wing test box using the co-curing technique (Fig. 14). Moisture losses for without



painting and sealing specimen clearly shows that percentage of moisture will not come down drastically even if some unavoidable circumferences the chamber breaks down minimum one week during moisture absorption period.

Full scale fatigue testing has been carried out on the flap structure with skin to stiffener debonds for the damage tolerance studies. The integrity of the composite flap structures having de-bonds or weak bonds at the rib skin interfaces under cyclic loading have been addressed. Resistance strain gauges, ultrasonic A-Scan, thermography and acoustic emission sensors are used to assess the damage growth during the test. Changes in strains during the damage growth are not significant as the growth of debonds is very small at many locations. Use of strain gauges did not help much because it is impossible to predict which debond grows during the test. So the choice of strain gauge locations is a tough task and totally arbitrary. Portable ultrasonic A-scan system is very useful to monitor the damage growth without removing the component from the test rig after every 1000 cycles. But the manual monitoring in A-scan needs careful inspection to find very small propagation around the existing debonds. Thermography revealed the growth in debonds after subjecting the component to fatigue load test. The scaled images from thermography helped to assess the growth of debonds precisely. It also helped to support the manual ultrasonic A-scan report. Acoustic emission monitoring proved to be extreme useful to monitor the health of structure online. From the test, it is found that the growth in any debond is discrete and intermittent. No continuous growth has been observed in any de-bond. The results have also shown that the damages have grown only to a small extent. These defects/damages have not altered the response of the structure either locally or globally. From the test, it can be concluded that the defects in the skin-stiffener bonding can sustain the 2 lacks of load cycles and will not result in a catastrophic failure between the inspection intervals. The test proves that the composite structures using co-bonding and secondary bonding have excellent fatigue resistance and damage tolerant. These test results give confidence to the designer to use the composite structures without much concern.

The load versus deflection and strain behavior of the elevator has been monitored during the test is discussed above. Accordingly, the plots have been prepared.

Deflections along the leading edge, spar line and trailing edge due to distributed loading were linear upto 150%. Maximum deflection recorded was 10.48 on the trailing edge. Strains at all locations were linear and maximum strain recorded was 4670 on the metallic Inner hinge link. Reaction load measured at the operating lever was 372 kg and the theoretical load expected was 363.3 kg. The test results and analysis results are compared and there is a good co relation between the test and FEM results. There is no permanent deformation in the component even though it undergone 198 % of limit load.

The test on wing test box has been conducted to prove the design of wing torsional box in the proposed composite wing for SARAS. The box has been subjected to the design ultimate load and the deflections, strains and AE response studied in detail. The results from the test and the analysis are compared and at majority of the locations, there is a good correlation between test and FEM results. No permanent deformations are observed in fasteners and fastener holes at skin and spar splice joints. The box withstood the ultimate load cases without any delamination or any major damage.

## **ACKNOWLEDGEMENTS**

Authors of this paper thank Director, National Aerospace Laboratories (NAL), Bangalore for his financial support to carry out this investigation. We also sincerely thank the support extended by the Head and Joint Head of Advanced Composite Division of NAL, Banaglore. Thanks to Thimmaiah and his teammates for the preparation and conducting the tests. We wish to thank Mr. Ashok Kumar and Mr. Jagadeeshan, for their technical support.

## **REFERENCES**

- [1] Review of Design Allowable for LCA Carbon Fibre Composites P.D. Mangalagiri PD CW 9201, NAL.
- [2] Meeks, Charlotte; Greenhalgh, Emile and Falzon, Brian G., "Stiffener Debonding Mechanisms in Post-Buckled CFRP Aerospace Panels", Composites Part A: Applied Science and Manufacturing, Vol. 36, Issue 7, July 2005, pp. 934–946.
- [3] Greenhalgh, Emile; Meeks, Charlotte; Clarke, Andrew and Thatcher, James, "The Effect of Defects on the Performance of Post-Buckled CFRP Stringer-

- Stiffened Panels”, *Composites Part A: Applied Science and Manufacturing*, Vol. 34, Issue 7, July 2003, pp. 623–633.
- [4] Freitas, M. de and Carvalho, R. de, “Residual Strength of a Damaged Laminated CFRP Under Compressive Fatigue Stresses”, *Composites Science and Technology*, Vol. 66, Issues 3–4, March 2006, pp. 373–378.
- [5] Yap, Jeff W.H., Scott, Murray L., Thomson, Rodney S. and Hachenberg, Dieter, “The Analysis of Skin-to-Stiffener Debonding in Composite Aerospace Structures”, *Composite Structures*, Vol. 57, Issues 1–4, July 2002, pp. 425–435.
- [6] Varughese, Byji, Subramanya, H.Y., Ramanaiah, B., Nagarajappa, N., Kotresh, Kamath, Ramesh Sundaram and Rao, M. Subba, “Damage Tolerance on Carbon Fibre Composite Flap Structures Having Defects at Rib-Skin Interfaces”, *Proceedings of ICASI-2004 International Conference on Advances in Structural Integrity*.
- [7] Chakravarthy, S. Bhaskar and Sakar, Bipul, Maximum Air Loads on the Control Surfaces and Tabs—A Compilation, Report No. SARAS/AERO/0069.
- [8] FEM Analysis of Saras Elevator S. Manju and R. Basavanna, PDST-9815.
- [9] Test Schedule for the Structural Static Testing of Wing Test Box for SARAS Aircraft, TS-20, Vol. 22, September 2007.
- [10] Stress Analysis of Composite Wing Test Box for SARAS Aircraft, DR-80, Vol. 03, December 2007.